JPMTR-2410
DOI 10.14622/JPMTR-2410
UDC 519.6:621.798:658.5:677.027

Scientific paper | 194
Received: 2024-01-17
Accepted: 2024-12-02

Retroactive effect of variable tensile forces on lateral web motion and lateral registration errors

Günther Brandenburg

Tölzer Str. 41, 82194, Gröbenzell, Germany gap.brandenburg@t-online.de

Abstract

The lateral position of a continuous web can be determined by a control roller at an angle to the longitudinal direction of web motion together with subsequent auxiliary rollers. However, a change in the tensile force changes this lateral position. The solution of the system of descriptive differential equations leads to a separate treatment of pure translation and pure rotation of the control roller. However, a resulting block plan for the dynamics of lateral motion was found, which is combined with the longitudinal mass flow and the retroactive effect of variable tensile forces on the lateral motion. Transverse and longitudinal register errors in the multi-roller system can be mapped together with the mass flow chain in the form of a multi-layer model. This enables extensive simulations of all system quantities as well as the design and optimization of control loops.

Keywords: lateral web motion, longitudinal mass flow chain, lateral and longitudinal register errors, variable tensile forces, retroactive effect, multi-layer model

1. Introduction

The subject of one of the last papers in this series was the two-dimensional registration error, which consists of the longitudinal and lateral registration errors (Brandenburg, 2023). A block diagram had been developed in which the mass flow is closely linked to the generation of the longitudinal registration error, while the lateral one was independent of the mass flow. This simplification does not correspond to physical reality, because changing web tensile forces influence the behavior of the side edges. In the contribution presented here, this dependency is taken into account in an extended model.

1.1 State of the art

In Brandenburg and Klemm (2016), Shelton's beam model (Shelton, 1968) was extended to variable web forces. Variable web forces are caused, apart from technological influences, by changes in the circumferential speeds of rollers that are provided for the transport and processing of the moving web. The equation of the beam bending and the so-called transport equations were linearized. Then additional dynamic terms were found that show the influence of a variable web tensile force during translational or rotational movement of a control roller as well as when a web offset or an angle change was impressed at the entrance to a system.

The numerical example from Brandenburg and Klemm (2016), Figure 6.1.2, led to plausible values of the lateral web deviations. However, it was not possible to verify these results by measurements because no printing press was available. Nevertheless, due to the mentioned plausibility, it makes sense to create a system plan supplemented by the retroactive effect, with the help of which numerous realistic simulations are possible. As in Brandenburg and Klemm (2023), a Bernoulli web is used.

2. Block diagram of the Bernoulli web

2.1 System of notation

In the following, the most important equations of Brandenburg and Klemm (2016; 2019) (in this case for the shear coefficient $a = 1$, valid for the Bernoulli web) are shown.

The system equations that describe the lateral dynamics of the web are the bending equation of the Bernoulli beam (or in the case of Brandenburg and Klemm (2019), the Timoshenko beam) and the two so-called transport equations (velocity equation and acceleration equation)

of the web. At constant transport velocity and constant stress, the bending equation of the Bernoulli beam according to Brandenburg and Klemm (2016), Equation (3.3.1) is

$$\frac{\partial^4 y(x,t)}{\partial x^4} - K_\mathrm{B}^2 \frac{\partial^2 y(x,t)}{\partial x^2} = 0 \qquad [1]$$

with the square of the curvature factor for the Bernoulli web (index 'B')

$$K_\mathrm{B}^2 = \frac{T}{EI} \qquad [2]$$

with

- T: tensile force in newtons [N], affecting beam deformation
- E: modulus of elasticity in pascals [Pa], indicating material stiffness
- I: area moment of inertia about the z-axis in [m^4], reflecting bending resistance.

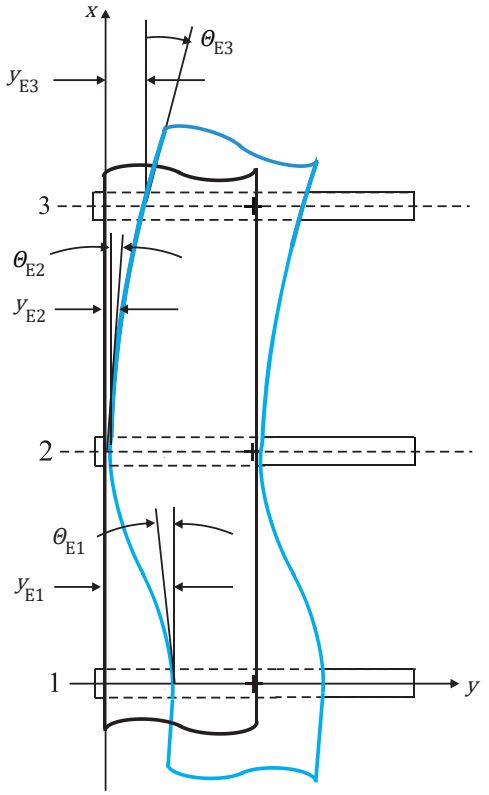

Figure 1: Mathematical notation system for a three-roller system with input offset and change of input angle at roller 1; quantities are given in the List of symbols

In order to introduce variable web velocities and variable tensile forces, Equation [1] must be linearized for small deviations (marked by tilde) from the steady state (marked by horizontal dash), since $K_\mathrm{B} = K_\mathrm{B}(t)$ is a time function now. Linearization was performed in Brandenburg and Klemm (2016).

The linearized form of the Bernoulli web is given by Brandenburg and Klemm (2016), Equation (6.1.4):

$$\frac{\partial^4 \tilde{y}(x,t)}{\partial x^4} - \bar{K}_\mathrm{B}^2 \frac{\partial^2 \tilde{y}(x,t)}{\partial x^2} = \kappa_\mathrm{m} \tilde{T}(t) \qquad [3]$$

with the mean curvature factor

$$\kappa_\mathrm{m} = \frac{1}{EI} \left(\frac{\partial^2 \bar{y}_E(x)}{\partial x^2} \right)_\mathrm{mean} \qquad [4]$$

and the curvature factor

$$\bar{K}_\mathrm{B}^2 = \frac{\bar{T}}{EI} \qquad [5]$$

at the steady-state operating point, as described by Brandenburg and Klemm (2016), Equations (6.1.9) and (2.1.8). Equation [3] is a linear, inhomogeneous differential equation with constant coefficients. This was solved in Brandenburg and Klemm (2016), by the method of variation of the constant (Lense, 1948).

2.2 Transfer functions of the Bernoulli web with variable tensile force and change of position of the control roller

A distinction must be made between two movements of the control roller, namely a pure translation and a pure rotation, because different boundary conditions apply to each of these movements as shown in Brandenburg and Klemm (2016), in Figure 3.3.1, a and b. Accordingly, even in the case of constant web force, there are two separate solutions of the homogeneous, linearized partial differential equation. In the case of variable tensile force, different dynamic terms consequently occur in the case of variable tractive force.

According to Brandenburg and Klemm (2016), Equation (6.3.11) presents the following Laplace-domain transfer function:

$$\tilde{y}_{\mathrm{E3,trans}}(s) = \frac{\frac{\tau_{23}^2}{\bar{f}_{\mathrm{B},23}} s^2 + \bar{K}_\mathrm{B} \tau_{23} s}{\frac{\tau_{23}^2}{\bar{f}_{\mathrm{B},23}} s^2 + \bar{K}_{\mathrm{B},23} \tau_{23} s + 1} \tilde{z}_2(s) + \frac{\frac{L_{23}^2}{\bar{f}_{\mathrm{B},23}} \frac{\mathcal{C}_{5,\mathrm{trans}}^{(23)} \kappa_{\mathrm{m},23}}{\bar{K}_{\mathrm{B},23}^2}}{\frac{\tau_{23}^2}{\bar{f}_{\mathrm{B},23}} s^2 + \bar{K}_{\mathrm{B},23} \tau_{23} s + 1} \tilde{T}_{23}(s) \qquad [6]$$

Equation [6] corresponds to web section 2–3 and assumes pure linear translation of the control roller. In this context, the index 'L' from Brandenburg and Klemm (2016) has been substituted with the web section identifier 23, as depicted in Figure 1. Additionally, Equation (6.3.4) from Brandenburg and Klemm (2016) applies

$$C_{5,\mathrm{trans}}^{(23)} = \left[f_{1T}\bar{K}_{\mathrm{B}}^2 \sinh\bar{u} + f_{2T}\bar{K}_{\mathrm{B}}^2 \cosh\bar{u} + (\cosh\bar{u} - 1)\right]_{23} \quad [7]$$

$\bar{K}_{\mathrm{B},23}^2 = \bar{T}_{23}/(EI)$ according to Equation [6] and Brandenburg and Klemm (2016), Equation (6.1.9), and $\bar{u} = \bar{u}_{23} = \bar{K}_{\mathrm{B},23} L_{23}$ after Brandenburg and Klemm (2019), Equation (3.26).

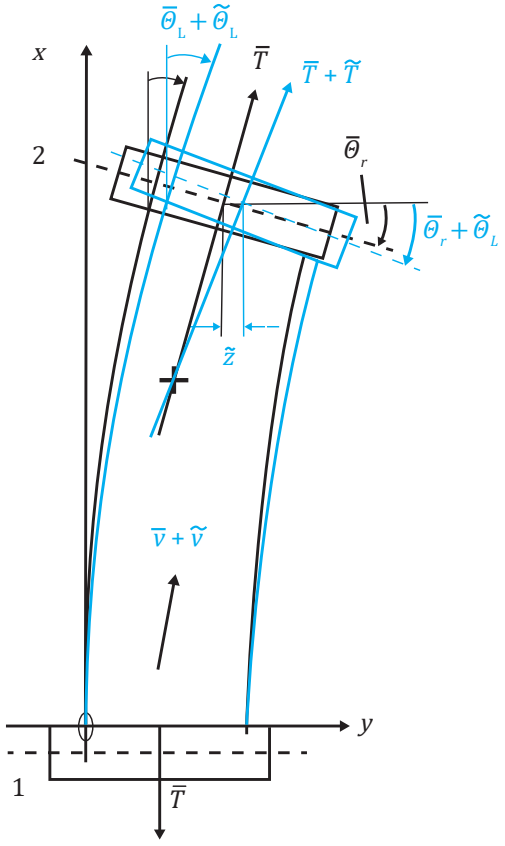

Figure 2: Steady state (black) and small deviations (blue) of the web (from Brandenburg (2016), Figure 6.1.1). Quantities are given in the list of symbols

Since the solution to the homogeneous differential equation (the first term on the right side of Equations [6] and [8]) aligns with the block plan, the second term on the right must also conform to it. This is because the linearized inhomogeneous bending equation from Brandenburg and Klemm (2016), Equation (6.1.10), is structurally composed of the same elements as the homogeneous bending equation in Equation (6.1.2).

The corresponding relations for pure rotation, as described in Brandenburg and Klemm (2016), Equation (6.3.14), are

$$\tilde{y}_{\mathrm{E3,rot}}(s) = \frac{\bar{K}_{\mathrm{B},23}}{\frac{\tau_{23}^2}{\bar{f}_{\mathrm{B},23}} s^2 + \bar{K}_{\mathrm{B},23}\tau_{23} s + 1} L_{23}\tilde{\Theta}_{\mathrm{r2}}(s) + \frac{\frac{L_{23}^2}{\bar{f}_{\mathrm{B},23}} \frac{C_{5,\mathrm{rot}}^{(23)}\kappa_{\mathrm{m},23}}{\bar{K}_{\mathrm{B},23}^2}}{\frac{\tau_{23}^2}{\bar{f}_{\mathrm{B},23}} s^2 + \bar{K}_{\mathrm{B},23}\tau_{23} s + 1} \tilde{T}_{23}(s) \quad [8]$$

with

$$C_{5,\mathrm{rot}}^{(23)} = \left[g_{1T}\bar{K}_{\mathrm{B}}^2 \sinh\bar{u} + g_{2T}, \bar{K}_{\mathrm{B}}^2 \cosh\bar{u} + (\cosh\bar{u} - 1)\right]_{23} \quad [9]$$

Both equations, [6] and [8], consist of the solution of the homogeneous linearized differential equation and of the new term of the change in tensile force.

Now it is necessary to determine at which point in the block plan the variable tensile force $\tilde{\Theta}_{\mathrm{r2}} = 0$ acts. In the first step, the double block plan of Figure 3 is drawn below. The upper part of the plan refers to the pure translation of the control roller, i.e. $\tilde{\Theta}_{\mathrm{r2}} = 0$, the lower part for the pure rotation of the control roller, i.e. $\tilde{z}_2 = 0$.

In the case of pure translation the simpler expression E_{z2} is introduced:

$$\tilde{y}_{\mathrm{E3}}(s) = E_{\mathrm{z2}} A_{23}(s)\tilde{T}_{23}(s) = \frac{1}{\frac{\tau_{23}^2}{\bar{f}_{\mathrm{B},23}} s^2 + \bar{K}_{\mathrm{B},23}\tau_{23} s + 1} E_{\mathrm{z2}}\tilde{T}_{23}(s) \quad [10]$$

with the retro-active factor (c.f. Brandenburg and Klemm (2016), Equation (6.3.12))

$$E_{\mathrm{z2}} = \frac{L_{23}^2}{\bar{f}_{\mathrm{B},23}} \frac{C_{5,\mathrm{rot}}^{(23)}\kappa_{\mathrm{m},23}}{\bar{K}_{\mathrm{B},23}^2} \quad [11]$$

In the case of pure rotation the simpler expression $E_{\theta 2}$ is introduced:

$$\tilde{y}_{\mathrm{E3}}(s) = E_{\theta 2} A_{23}(s)\tilde{T}_{23}(s) = \frac{1}{\frac{\tau_{23}^2}{\bar{f}_{\mathrm{B},23}} s^2 + \bar{K}_{\mathrm{CB},23}\tau_{23} s + 1} E_{\theta 2}\tilde{T}_{23}(s) \quad [12]$$

with the retro-active factor

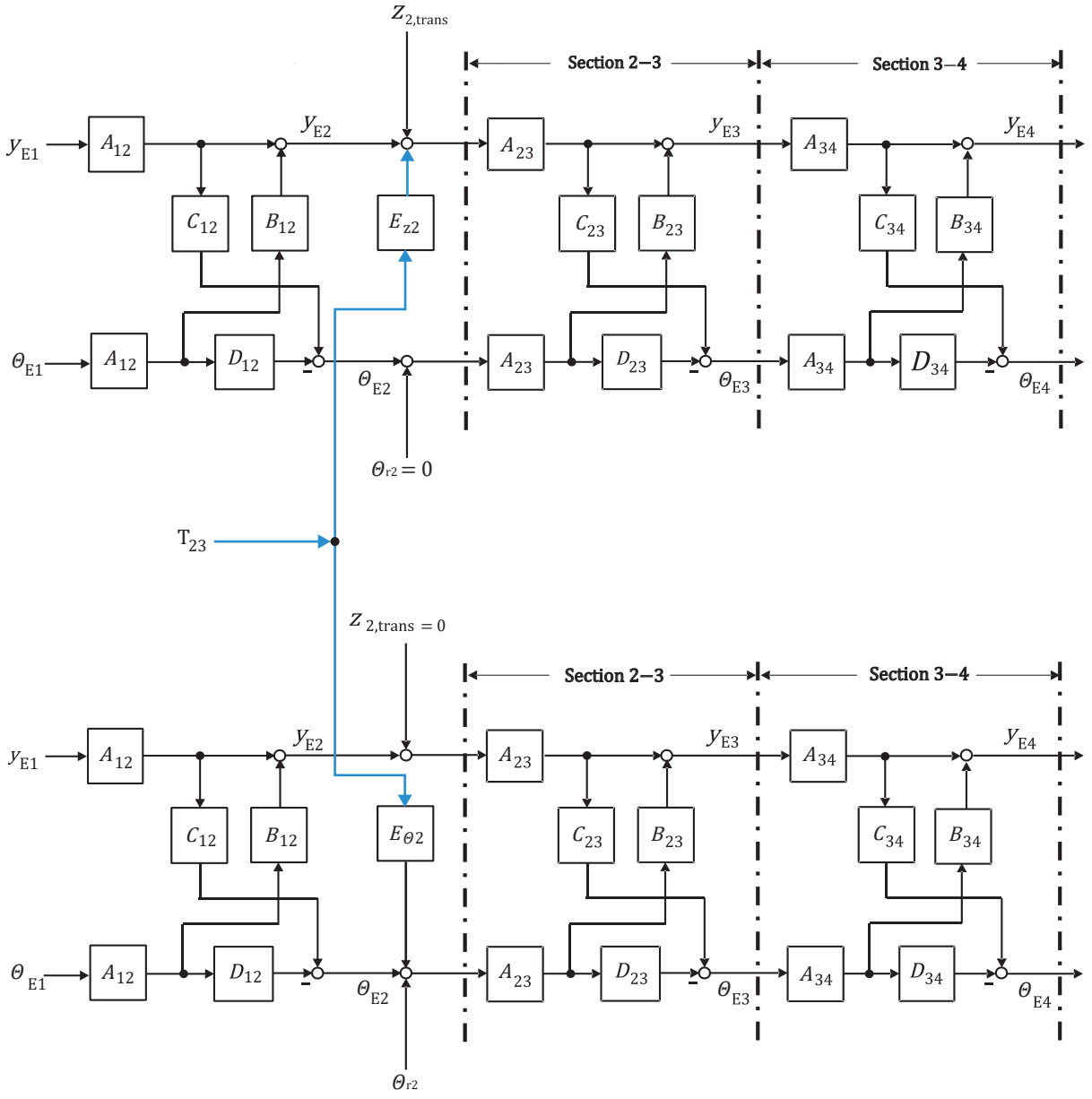

Figure 3. Changes in tensile force (blue) according to the block plan in Brandenburg and Klemm (2019), Figure 5.12; the upper partial block plan is used for pure translation, the lower one for the pure rotation of the control roller; all variables are small deviations from the steady state; quantities are presented in the list of symbols

$$E_{\Theta 2} = \frac{L_{23}^2}{f_{\mathrm{B},23}} \frac{C_{5,\mathrm{rot}}^{(23)} \kappa_{\mathrm{m},23}}{\bar{K}_{\mathrm{B},23}^2} \qquad [13]$$

These terms are shown in Figure 3.

2.3 Transfer functions for input offset and angle change

An input offset and/or a change in input angle were not addressed in Brandenburg and Klemm (2016).

2.3.1 Input offset

If an input offset $\tilde{y}_{E1}$ occurs at roller 1 (see Brandenburg and Klemm (2019), Figure 4.1), and the control roller is in the rest position ($\tilde{z}_2 = \tilde{\Theta}_{r2} = 0$) the input offset is propagated to the entry of roller 2 and triggers both an input offset $\tilde{y}_{E2}$ and a change in the input angle $\tilde{\Theta}_{E2}$.

The upper partial block plan of Figure 3 shows the following: A pure translation $\tilde{z}_{2,\mathrm{trans}}$ dynamically results in

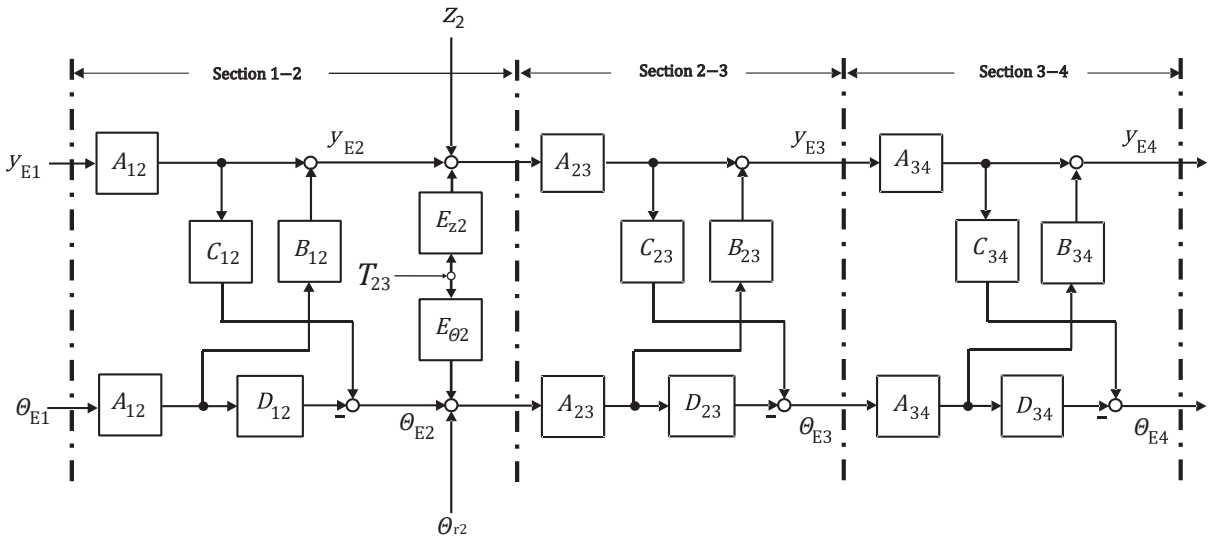

Figure 4. Web tensile force at the summation points of z2 = $z_{(2,\mathrm{trans})}$ and $\Theta_{r2} = \Theta_{(r2,rot)}$. Quantities are presented in the list of symbols

the same dynamic reaction in section 2–3 as an input offset in section 1–2. Therefore, the same equations apply universally, but with appropriately modified transfer blocks. Analogous to Brandenburg and Klemm (2016), Equation (6.3.11), it is written:

$$\tilde{y}_{\mathrm{E2,Evers}}(s) = \frac{\frac{\tau_{12}^2}{f_{\mathrm{B}}(\bar{u})}s^2 + \bar{K}_{\mathrm{B}}\tau_{12}s}{\frac{\tau_{12}^2}{f_{\mathrm{B}}(\bar{u})}s^2 + \bar{K}_{\mathrm{B}}\tau_{12}s + 1}\tilde{y}_{\mathrm{E1,Evers}}(s) + \frac{\frac{L_{12}^2}{f_{\mathrm{B}}(\bar{u})}\frac{\underline{C}_{5,\mathrm{Evers}}^{(12)}\kappa_{\mathrm{m}}}{\bar{K}_{\mathrm{B}}^2}}{\frac{\tau_{12}^2}{f_{\mathrm{B}}(\bar{u})}s^2 + \bar{K}_{\mathrm{CB}}\tau_{12}s + 1}\tilde{T}_{12}(s) \quad [14]$$

$$\underline{C}_{5,\mathrm{Evers}}^{(12)} = \left[f_{1T}\bar{K}_{\mathrm{B}}^2\sinh\bar{u} + f_{2T}\bar{K}_{\mathrm{B}}^2\cosh\bar{u} + (\cosh\bar{u} - 1)\right]_{12} \quad [15]$$

and $\bar{K}_{\mathrm{B}}^2$ according to Equation [3]. The first term on the right indicates that for $t \to \infty$ the input offset has arrived at the input of roller 2. The second term describes the influence of the variable tensile force on the input of roller 2 and comes from Brandenburg and Klemm (2016), Equation (6.3.11), and Equation [14] is identical to the second term of Brandenburg and Klemm (2019), Equation (4.83) when formulated for the Bernoulli web.

2.3.2 Change of the input angle

The following can be seen in the lower partial block plan of Figure 3: A pure change in angle $\tilde{\Theta}_{\mathrm{r2}}$ results in the same dynamic reaction in section 2–3 as a change in the input angle $\tilde{\Theta}_{E1}$ for section 1–2. Therefore, the same equations apply, but with modified transfer blocks. Analogous to Equation (6.3.14) in Brandenburg and Klemm (2016) it is written:

$$\tilde{y}_{\mathrm{E2,Ewinkel}}(s) = \frac{\bar{K}_{\mathrm{B}}(\bar{u})}{\frac{\tau_{12}^2}{f_{\mathrm{B}}(\bar{u})}s^2 + \bar{K}_{\mathrm{B}}(\bar{u})\tau_{12}s + 1} \times L_{12}\tilde{y}_{\mathrm{E1,Ewinkel}}(s) + \frac{\frac{L_{12}^2}{f_{\mathrm{B}}(\bar{u})}\frac{\underline{C}_{5,\mathrm{Ewinkel}}^{(12)}\kappa_{\mathrm{m}}}{\bar{K}_{\mathrm{B}}^2}}{\frac{\tau_{12}^2}{f_{\mathrm{B}}(\bar{u})}s^2 + \bar{K}_{\mathrm{B}}(\bar{u})\tau_{12}s + 1}\tilde{T}_{12}(s) \quad [16]$$

with

$$\underline{C}_{5,\mathrm{Ewinkel}}^{(12)} = \left[g_{1T}\bar{K}_{\mathrm{B}}^2\sinh\bar{u} + g_{2T}\bar{K}_{\mathrm{B}}^2\cosh\bar{u} + (\cosh\bar{u} - 1)\right]_{12} \quad [17]$$

Then the two partial block plans from Figure 3 can be pushed one on top of the other to create Figure 4, in which the change in tensile force $\tilde{T}_{23}(s)$ acts in the middle between the blocks E_{z2} and $E_{\theta 2}$. In the model according to Brandenburg and Klemm (2019), Figure 5.5, it is assumed that when the input offset and/or input angle change is assumed, the control roller 2 (see Figure 5) is in the rest position.

The question of what kind of transient would occur if the control roller is at rest but at an angle, i.e. has a stationary position $\bar{\Theta}_{\mathrm{r2}} \neq 0$, is not relevant. This is because

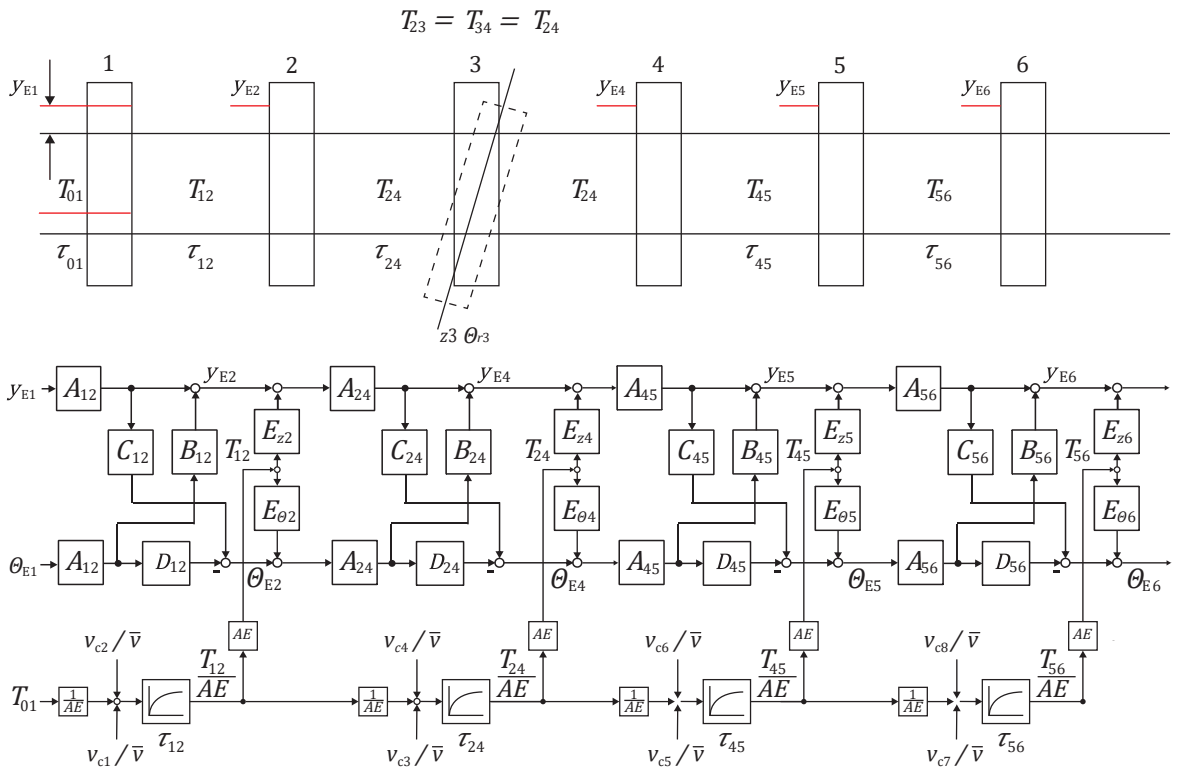

Figure 5: Complete system with control roller and mass flow chain; all variables are small deviations from the steady state; quantities are presented in the list of symbols

it is an initial state that influences the stationary movement of the web, but which no longer plays a role after the introduction of small deviations.

2.4 Relationship of tensile force with the continuity equation

2.4.1 Transfer functions of the lateral behavior under the influence of control rollers

The following consideration is important: The three-roller system in Figure 1 assumes that there is a change in tensile force $\tilde{T}$ on roller 2, which is accompanied by a change in the speed of the web. The main reason for this is not important for this particular discussion.

2.4.2 Mass flow in the six-roller system and reaction to lateral movement

So far, the causes of a change in web force have not been discussed, but rather how this affects lateral web deviation has been investigated.

Changes in web tension and web force are – apart from changes in humidity and temperature – caused by the mass flow, for example by changing the peripheral speeds of the drive rollers, as is well known. The mathematical description is based on the continuity equation. This concept was already derived in Brandenburg (1976). In contrast to German literature, it has hardly played a role in American engineering literature. Anyhow, in recent years, interest in applying these principles to high-speed web handling has grown.

For Bernoulli webs, i.e. webs that are not too wide ($L/b > 10$, where L is the length and b the width of the web, i.e. by definition its shear factor is $a = 1$) can be shown that:

- The equations of the lateral behavior of the web and the mass flow are only slightly coupled to one another,
- There is hardly any difference between the continuity equation in the x-direction and the slightly different lateral transport direction.

A six-roller system according to Figure 5 with control roller 3 is assumed. In this case, the mass flow chain drawn in Figure 6 follows from Equation [18].

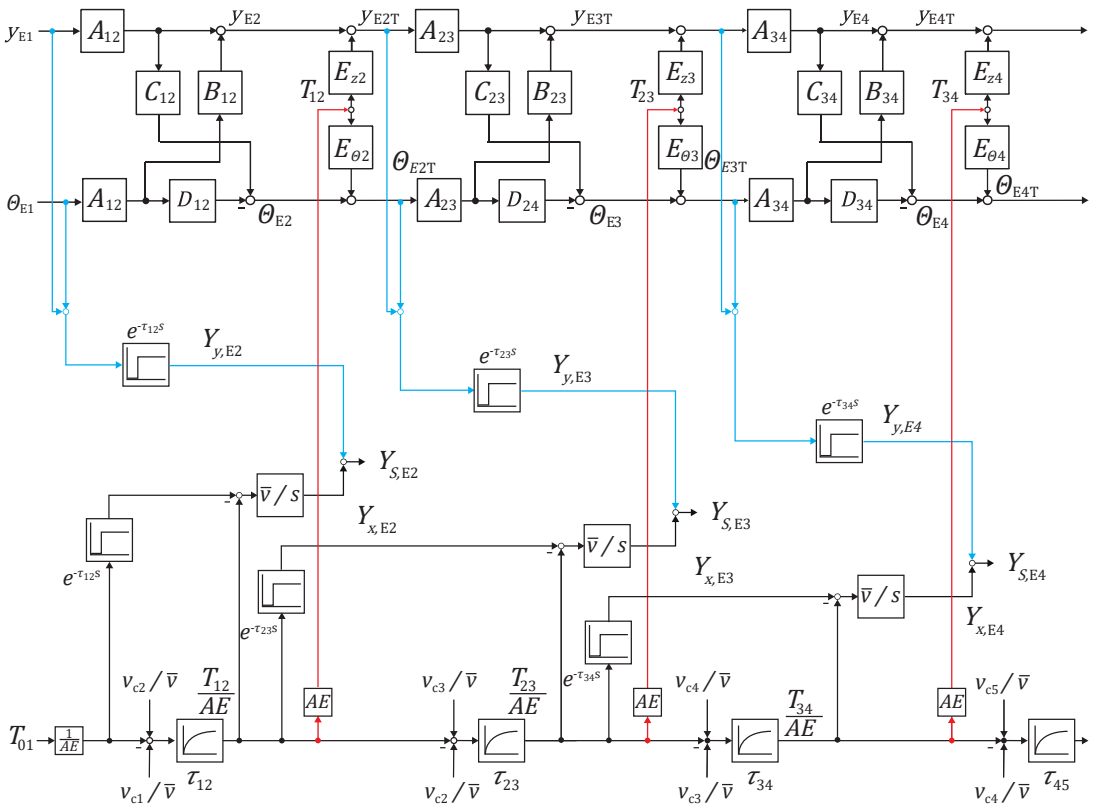

Figure 6: Block plan of the overall system without control roller (blue signal lines: lateral register errors, black signal lines: longitudinal register errors, red signal lines: retroactive effect of the web tensile forces); ; quantities are presented in the list of symbols

$$\tilde{\varepsilon}_{i,i+1}(s) = \frac{1}{1+\tau_{i,i+1}s} \times \left[\tilde{\varepsilon}_{i,i-1}(s) + \frac{\tilde{v}_{c,i+1}(s) - \tilde{v}_{c,i-1}(s)}{\bar{v}}\right] \quad [18]$$

The tensile force $\tilde{T}_{01}$ is impressed on the roller 1. The control roller 3 is positioned between the axially driven rollers 2 and 4. The rollers 5 and 6 are also axially driven rollers. Each web section is represented by a PT1 element (i.e. a 1st order lag) with a time constant according to Equation [18]. These PT1 elements act on the lateral deflection and the angular deviation of the actual web.

The strain was written in the form

$$\tilde{\varepsilon}_{i,i+1} = \frac{\tilde{T}_{i,i+1}}{AE} \quad [19]$$

Since the movement of the control roller has no influence on the web tension, the web tension in sections 2–3 and 3–4 is the same. The question now is whether every lateral deviation $\tilde{y}_{Ei}$ and every change in angle $\tilde{\Theta}_{Ei}$ can be assigned a reaction from the material flow chain. The answer is that this is mandatory. For example, it may be that $\tilde{T}_{01} = 0$ and only the speed $\tilde{v}_{c5} \neq 0$ changes. Then there is always a reaction on $\tilde{y}_{E5}$ and $\tilde{\Theta}_{E5}$ (see Figure 5).

The next step is to add the register errors to the block plan from Figure 5.

2.5 Registration errors taking into account the retro-active effects of variable web tensile forces

In the publication Brandenburg and Klemm (2023), Figure 4, there is already a system plan with lateral and longitudinal registration errors, which, however, does not take into account the effects of changes in tensile force on the lateral behavior of the web. Figure 5 presented here has been supplemented with the additional blocks of register errors, without the control roller for reasons of clarity. This creates the 'multi-layer plan' presented in Figure 6.

In the 'cycle' of the mass flow chain, the lateral web deviations and thus the lateral register errors are influenced via the signal paths marked in red.The longitudinal register errors due to the force changes in the mass flow chain are well known. When adding the longitudinal and the lateral register error, it must be noted that the two

errors are perpendicular to each other (Brandenburg and Klemm, 2023).

If the mass flow chain is only excited by $\widetilde{T}_{01}$, the three longitudinal register errors $\widetilde{Y}_{x,\mathrm{E2}}$, $\widetilde{Y}_{x,\mathrm{E3}}$ and $\widetilde{Y}_{x,\mathrm{E4}}$ appear. The retro-active signal paths (red in Figure 5) produce the lateral register errors $\widetilde{Y}_{y,\mathrm{E3}}$ and $\widetilde{Y}_{y,\mathrm{E4}}$, without any change in $\widetilde{y}_{\mathrm{E1}}$ or $\widetilde{\Theta}_{\mathrm{E1}}$. The lateral register error $\widetilde{Y}_{y,\mathrm{E2}}$ also occurs, only if $\widetilde{y}_{\mathrm{E1}} \neq 0$ and/or $\widetilde{\Theta}_{\mathrm{E1}} \neq 0$ is valid.

The following engineering and scientific results are completely new.

The multi-layer model of Figure 6 did not yet exist in this form. It consists of three layers, which can be characterized as follows:

1) In the upper layer, it shows the linkage of the lateral deflections and input angle changes according to the lateral block plan.

2) In the lower layer it shows the link of the longitudinal strain changes $\varepsilon_{i,i+1} = \widetilde{T}_{i,i+1}/(AE)$ with the peripheral velocities of the longitudinal time lags. And it is an image of the mass flow.

3) The middle layer consists of the lateral register errors $\widetilde{Y}_{y,\mathrm{E}}$ and the longitudinal register errors $\widetilde{Y}_{x,\mathrm{E}}$.

Their sum makes up the total register errors $\vec{\widetilde{Y}}_{S,\mathrm{E}}$. When adding, it should be noted that they are spatially perpendicular to each other. Therefore, they can also be written vectorially, as Equation [20] shows (Brandenburg and Klemm, 2023):

$$\vec{\widetilde{Y}}_{S,\mathrm{E}i} = \vec{\widetilde{Y}}_{x,\mathrm{E}i} + \vec{\widetilde{Y}}_{y,\mathrm{E}i} = \widetilde{Y}_{x,\mathrm{E}i}\vec{e}_x + \vec{\widetilde{Y}}_{y,\mathrm{E}i}\vec{e}_y \qquad [20]$$

This sum vector changes its magnitude and angle during a transient while the web is moving.

The multi-layer model shown in Figure 6 can be regarded as a new module of the automation technology.

2.6 Potential of the multi-level model

The multi-level model shown in Figure 6 offers a comprehensive application potential for simulations and subsequent measurements:

- Change of one or all three input variables: web offset, input angle and tensile force,
- Change of peripheral velocities of the mass flow chain and investigation of their effect on the other variables of the overall system,
- Extension of Figure 6 to include the partial cutting register errors (Brandenburg, 2011),
- Insertion of the mathematical models for doubling in and between printing units (Brandenburg 2000),
- Extension of Figure 6 by the electronic line shaft of the controlled drive motors,
- Insertion of side edge controls of the web,
- Insertion of the controls for longitudinal and/or lateral register errors,
- Non-interacting control of web forces and cut-off register errors in rotary printing presses with electronic line shafts (see Brandenburg, Geißenberger and Klemm, 2004),
- Investigation of controls of tensile forces.

3. Conclusion

The state-of-the-art printing press is a system consisting of printing units that print information on the moving web and of electric drive motors in the form of an electronic line shaft. Together with guide rollers these units provide high-precision longitudinal and lateral web guidance. Because of multiple disturbances, longitudinal and lateral register errors occur. In order to keep these register errors to a minimum, the disturbances must be minimized on the one hand by technological measures and on the other hand by means of closed-loop controls.The multi-layer model in Figure 6 shows the overall system of lateral and longitudinal register errors in a clear manner as well as the retro-active effect of the mass flow chain on the lateral register errors. The multi-layer model enables extensive simulations of the relevant system variables with the aim of reducing time-consuming measurements on real printing machines. In the case of printing companies with large pressroom equipment, e.g. with machines for commercial printing, machines for newspaper printing, and rotogravure presses for high-quality art printing, the multi-layer model, together with other production elements, could be fed into an AI that carries out higher-level operational coordination tasks (see also Chen, 2023).

Acknowledgement

I would like to express my sincere thanks to Dr. Andreas Klemm for carrying out the formatting guidelines and for fruitful discussions over many years for numerous publications.

List of symbols

a	Shear coefficient
b	Width of the web
$\underline{C}^{(23)}_{5,\mathrm{trans}}$, $\underline{C}^{(23)}_{5,\mathrm{rot}}$	Constants for pure translation and pure rotation, respectively, in web section 2–3 according to Equations [7] and [9]
E	Modulus of elasticity
E_{z2}	Retro-active factor of tensile force on the lateral web deflection, Equation [11]
$E_{\Theta 2}$	Retro-active factor of tensile force on the lateral web angle change, Equation [13]
$\bar{f}_{\mathrm{B},i,i+1}$	Steady state constant of the Bernoulli web in section $i, i+1$, Equations [6] and [8]
f_{1y}, f_{2y}	Constants according to Brandenburg and Klemm (2016), Equations (3.3.1.6), (3.3.1.7) and (6.2.6)
f_{1T}, f_{2T}	Constants according to Brandenburg and Klemm (2016), Equations (6.2.9) and (6.2.10)
g_{1T}, g_{2T}	Constants according to Brandenburg and Klemm (2016), Equations (6.2.18) and (6.2.19)
$g_{1\Theta}, g_{2\Theta}$	Constants according to Brandenburg and Klemm (2016), Equations (6.2.18) and (6.2.19)
h	Thickness of the web
I	Moment of inertia of area referred to the z-axis in [m^4]
K_{B}	Curvature factor $K = \sqrt{T/EI}$ in [m^{-1}] for the Bernoulli web
$K_{\mathrm{B},i,i+1}$	Curvature factor (of the Bernoulli web) in section $i, i+1$
$\bar{K}_{\mathrm{B}}$	Steady state curvature factor according to Brandenburg and Klemm (2016), Equation (2.1.8) and Equation [5]
$L_{i,i+1}$	Length of the free web between rollers $i, i+1$
s	Laplace transform operator
t	Time
T	Tensile force [N] according to Brandenburg and Klemm (2016), Figure 2.1.2
$\tau_{i,i+1}$	Time constant of the web in section $i, i+1$
$\widetilde{T}_{23}(s)$	Small variation of tensile force in section 2-3
$\bar{u}_{i,i+1}$	From curvature factor and length: $\bar{u}_{L,i,i+1} = \bar{K}_{\mathrm{B},i,i+1} L_{i,i+1}$ in web section $i, i+1$, according to Brandenburg and Klemm (2019), Equation (3.26) in steady state of motion
V	Velocity in direction of web motion (see Brandenburg and Klemm (2016), Figure 2.1.1)

$V_{\mathrm{C}} = v_{\mathrm{C}} \approx V$	Peripheral velocity of the control roller 2 (velocity of the web elements in the adhesion zone of the control roller ≈ web velocity, see Figure 2.1.1, Shelton 1968)
(x, y)	Coordinate system (see Figure 1)
y_{E}	Lateral web deflection (see Figure 1)
$y_{\mathrm{E}i,\mathrm{trans}}$	Lateral web deflection at entry i with translatory movement
$y_{\mathrm{E}i,\mathrm{rot}}$	Lateral web deflection at entry i with rotational movement
$y_{\mathrm{E2,Evers}}$	Lateral web deflection at entry i with input offset
$y_{\mathrm{E2,Ewinkel}}$	Lateral web deflection at entry i with change of the input angle
$\widetilde{Y}_{x,\mathrm{E}i}$	Longitudinal registration error at entry of roller i (see Figure 6)
$\widetilde{Y}_{y,\mathrm{E}i}$	Lateral registration error at entry of roller i (see Figure 6)
$\widetilde{Y}_{S,\mathrm{E}i}$	Lateral registration error (cf. Figure 6 and Equation [20])
z	Lateral position of roller 2 (see Figure 2)
Θ_{E}	Entry angle (see Figure)
Θ_L	Angle of web edge relative to x-axis at the entrance line of roller 2 (see Figure 2)
Θ_{r}	Rotation angle of the control roller (see Figure 4)

References

Brandenburg, G. and Tröndle, H.-P., 1976a. Dynamik des Längsregisters bei Rollenrotationsdruckmaschinen: Teil 1. *Siemens Forschungs- und Entwicklungsberichte*, 5(1), pp. 17–20.

Brandenburg, G. and Tröndle, H.-P., 1976b. Dynamik des Längsregisters bei Rollenrotationsdruckmaschinen: Teil 2. *Siemens Forschungs- und Entwicklungsberichte*, 5(2), pp. 65–71.

Brandenburg, G., 2000. Dynamisches Verhalten von Dublier- und Registerfehlern bei Rollenoffset Druckmaschinen. In: *Tagungsband SPS/IPC/DRIVES 2000*. Nürnberg, Germany, 28–30 November 2000. Heidelberg: Hüthig-Verlag, pp. 698–715.

Brandenburg, G., Geißenberger, S. and Klemm, A., 2004. Noninteracting control of web forces and cut-off register errors in rotary printing presses with electronic line shafts. In: *11th Int. Power Electronics and Motion Control Conference EPE-PEMC*. Riga, Latvia, Vol. 6, pp. 6-35 to 6-42.

Brandenburg, G., 2011. Advanced process models and control strategies for rotary printing presses. In: *Proceedings of the 11th International Conference on Web Handling*. Stillwater, OK, USA, 12–15 June 2011. Stillwater: Oklahoma State University.

Brandenburg, G. and Klemm, A., 2016. Lateralverhalten kontinuierlicher elastischer Bahnen, Kurzfassung des Balkenmodells von Shelton und Erweiterung auf variable Bahnzugkraft. In: U. Fügmann, ed. 2016. *Proceedings zum 13. Bahnlaufseminar,* Chemnitz, Germany, 19–20 September 2016. Berlin: VWF Verlag für Wissenschaft und Forschung 2017. pp. 35–104.

Brandenburg, G. and Klemm, A., 2019. Lateralverhalten elastischer Bahnen bei Berücksichtigung des Schubeinflusses. In: U. Fügman, ed. *Modellbildung und Simulation: Proceedings zum 14. Bahnlaufseminar 2018*. Chemnitz, Germany, 18–19 September 2018. Berlin: VWF Verlag für Wissenschaft und Forschung, pp. 53–150.

Brandenburg, G., 2023. Two-dimensional register error. *Journal of Print and Media Technology Research*, 12(3), 127–133. https://doi.org/10.14622/JPMTR-2303.

Chen, Z., 2023. Control of high precision roll-to-roll printing systems. PhD., University of Michigan, Horace H. Rackham School of Graduate Studies. https://doi.org/10.7302/8576.

Lense, J., 1948. Vorlesungen über höhere Mathematik. München, Leibnitz Verlag.

Shelton, J. J., 1968. Lateral dynamics of a moving web. PhD., Oklahoma State University, Stillwater, OK, USA.